



Research Article

New Approach of the Oxidant Peroxo Method (OPM) Route to Obtain $\text{Ti}(\text{OH})_4$ Nanoparticles with High Photocatalytic Activity under Visible Radiation

André E. Nogueira ^{1,2}, Lucas S. Ribeiro,³ Luiz F. Gorup,⁴ Gelson T. S. T. Silva,² Fernando F. B. Silva,² Caue Ribeiro ², and Emerson R. Camargo³

¹Brazilian Nanotechnology National Laboratory (LNNano), Brazilian Center for Research in Energy and Materials (CNPEM), Zip Code 13083-970 Campinas, São Paulo, Brazil

²National Laboratory of Nanotechnology for Agrobusiness (LNNA), EMBRAPA-Brazilian Agricultural Research Corporation, Rua XV de Novembro, 1452, São Carlos, SP 13560-970, Brazil

³Interdisciplinary Laboratory of Electrochemistry and Ceramics (LIEC), Department of Chemistry, Federal University of São Carlos, Rod. Washington Luis km 235, CP 676 São Carlos, SP 13565-905, Brazil

⁴FACET-Department of Chemistry, Federal University of Grande Dourados, Dourados, Mato Grosso do Sul 79804-970, Brazil

Correspondence should be addressed to André E. Nogueira; andreesteves86@hotmail.com

Received 12 June 2018; Revised 9 August 2018; Accepted 15 August 2018; Published 9 October 2018

Academic Editor: Juan M. Coronado

Copyright © 2018 André E. Nogueira et al. This is an open access article distributed under the Creative Commons Attribution License, which permits unrestricted use, distribution, and reproduction in any medium, provided the original work is properly cited.

Environmental problems related to the generation of wastewater contaminated with organic compounds and the emissions of pollutants from fuel burning have become major global problems. Thus, there is a need for the development of alternative and economically viable technologies for the remediation of the affected ecosystems. Therefore, this work describes the preparation and characterization of a $\text{Ti}(\text{OH})_4$ catalyst with the modified surface for application in the photodegradation of organic compounds (methylene blue (MB) dye and the drug amiloride (AML)) and in the artificial photosynthesis process. Characterization results reveal that peroxo groups on the surface of the catalyst had a great influence on the optical properties of the $\text{Ti}(\text{OH})_4$ and consequently in its photocatalytic property. This catalyst showed a high photocatalytic activity for the degradation of organic pollutants under visible radiation, reaching approximately 98% removal of both the dye and the drug in 150 min of reaction. In addition, the catalyst presented a great potential for the reduction of CO_2 under ultraviolet (UV) radiation when compared to P25, which is a classic catalyst used in photocatalytic processes. The highest photocatalytic activity can be attributed to the strong visible light absorption, due to the narrow band gap, and the effective separation of photogenerated electron-hole pairs caused by the peroxo groups on the $\text{Ti}(\text{OH})_4$ surface.

1. Introduction

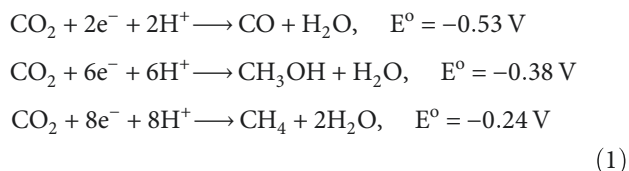
Photoactivated processes are receiving enormous attention due to important applications as solar cells, CO_2 photoreduction, water splitting for hydrogen production, for the degradation of organic compounds, and others [1, 2]. During these processes, semiconductors are irradiated with UV or visible radiation to excite electrons from the valence band (VB) to the conduction band (CB) creating electron/hole pairs. Most of the pairs recombine, but the remaining, via

oxidation-reduction reactions, promote the oxidation of water, producing hydroxyl radicals (OH^\cdot) from the positive holes in the VB and superoxide anions (O_2^-) from the electrons in the CB. In addition, the electrons in the CB can reduce the carbon dioxide (CO_2) generating hydrocarbons with a greater added value. These powerful oxidant radicals react with organic and toxic compounds, converting them to water, carbon dioxide, and other simple substances [3, 4].

In the photocatalytic process, two events can occur simultaneously: one involves the oxidation of adsorbed water

in the photogenerated holes in the VB, generating hydroxyl radicals (OH[•]) that have a high oxidation power of organic compounds and the second is related to the reduction of an acceptor of electrons (usually dissolved O₂ or CO₂) that were excited to CB.

The photogenerated electrons in the CB react with CO₂, reducing them to carbon monoxide, methane, ethanol, etc. [5].



This catalytic CO₂ photoreduction process, also called artificial photosynthesis, is a branch of heterogeneous photocatalysis.

The most widely used semiconductor in photocatalytic processes is TiO₂; however, due to its wide band gap (3.2 eV for the anatase phase), it can be activated only by near-UV light ($k < 385$ nm), which represents a small fraction of solar light (about 3–4%). The inactivity under visible light strongly limits the practical application of the TiO₂ photocatalyst [6]. In recent years, much research has been focused on improving the photocatalytic property of TiO₂, trying to minimize the two main drawbacks associated to the use of TiO₂: (i) high electron and hole recombination rates and (ii) low efficiency under visible irradiation [7].

In order to utilize visible light from solar energy and enhance the photocatalytic reactions, efforts have been focused on exploring novel methods to modify semiconductors such as the process of doping, sensitization, and formation of heterostructures [8]. Photosensitization can be achieved by a photosensitizer that absorbs light energy transforming it into chemical energy, which is transferred to substrates under favorable conditions. The photosensitizers may be adsorbed on the semiconductor surface by an electrostatic or chemical interaction and, upon excitation, inject electrons into the conducting band of the semiconductor. Based on the reported studies in the literature, organic dyes and coordination metal complexes are very effective sensitizers [9–11].

In this work, the OPM route was used with a new approach to obtain nanoparticles of Ti(OH)₄ with peroxo groups on the surface, in which its photocatalytic activity was evaluated both in the degradation process of the methylene blue dye and the amiloride drug, and in the process of CO₂ photoreduction, with particular emphasis on the effect of the groups on the optical properties and the photocatalytic efficiency of the catalyst.

2. Materials and Methods

2.1. Synthesis. The synthesis of the catalysts was based on the oxidant peroxo method (OPM) developed by Ribeiro et al. and Camargo et al., in which 250 mg of metallic titanium (98% Aldrich, USA) was added to 100 mL of a 3:2 H₂O₂/NH₃ (Synth, Brazil) aqueous solution, which was left in an

ice-water cooling bath until complete dissolution of metal, resulting in a transparent yellow solution of the soluble peroxytitanate complex [12–14]. The peroxytitanate complex solution was then heated to 80°C under stirring until the formation of a yellow gel that was dried at 60°C for 24 h to form the Ti(OH)₄ with the surface modified with the peroxo group. The Ti(OH)₄ was calcined at different temperatures between 300 and 500°C for 1 h at a heating rate of 10°C min⁻¹ in closed alumina boats. The different samples calcined 300, 400, and 500°C are referred as TiO₂-300°C, TiO₂-400°C, and TiO₂-500°C, respectively.

2.2. Characterization. The XPS spectra were performed using an XPS VG Microtech ESCA 3000 (MgK α and AlK α radiations) at an operating pressure of $3 \cdot 10^{-10}$ mbar. The binding energies were corrected for the charging effect by assuming a constant binding energy for the adventitious O1s peak. The LabRAM microspectrometer (HORIBA JobinYvon) was used to obtain the Raman spectra of the catalysts. The excitation wavelength was a 514.5 nm line of a 5.9 mW He-Ne laser as the excitation source is through an Olympus TM BX41 microscope. Thermogravimetric analysis of the catalyst was carried out using a TGA Q500 thermogravimetric analyzer (TA Instruments, New Castle, DE) in air flow and recorded from room temperature to 600°C, at a constant heating rate of 10°C/min. The Ti(OH)₄ was characterized by differential scanning calorimetry (DSC 404C controlled by TASC 424/3A, Netzsch, Germany) between 25 and 550°C using an aluminum crucible and a constant heating/cooling rate of 10°C/min with a flux of 0.50 cm³/min. A Rigaku D/MAX 200 diffractometer was used to determine crystal structure of the catalysts, with CuK α radiation and scanned for 2θ values from 5 to 80°. Infrared absorption spectra were recorded by a Fourier transform infrared spectrometer (FTIR) (Bruker EQUINOX 55, Ettlingen, Germany). Spectra were recorded for KBr disks containing a powdered sample and obtained in the 400–1000 cm⁻¹ range, with 64 scans and 4 cm⁻¹ resolution. The surface morphology of the catalysts was observed by field emission scanning electron microscopy (FESEM, ZEISS model-SUPRA 35). The band gap of the catalysts was determined according to the method proposed by Wood and Tauc [15] and Tolvaj et al. [16]. The spectra were recorded using the UV-visible diffuse reflectance spectroscopy (DRS) at room temperature between 200 and 800 nm using a Varian model Cary 5G in the diffuse reflectance mode (R). The specific surface areas of the catalysts were measured with a Micromeritics ASAP-2020 instrument and calculated by the Brunauer-Emmett-Teller (BET) method. The catalysts were pretreated (degassing) by heating at 70°C under vacuum until reaching a degassing pressure of less than 20 mmHg.

2.3. Photodegradation. The photocatalytic activity of the catalyst was evaluated using twenty milliliters of a 10 mg L⁻¹ solution of MB dye or AML drug, mixed with 10 mg of the catalyst, and irradiated with visible (six 15 W Osram lamps, with maximum intensity at 440 nm) and UV (six 15 W Phillips TUV UVC lamps, with maximum intensity at 254 nm) light inside a thermostated photoreactor at $25 \pm 3^\circ\text{C}$. To investigate

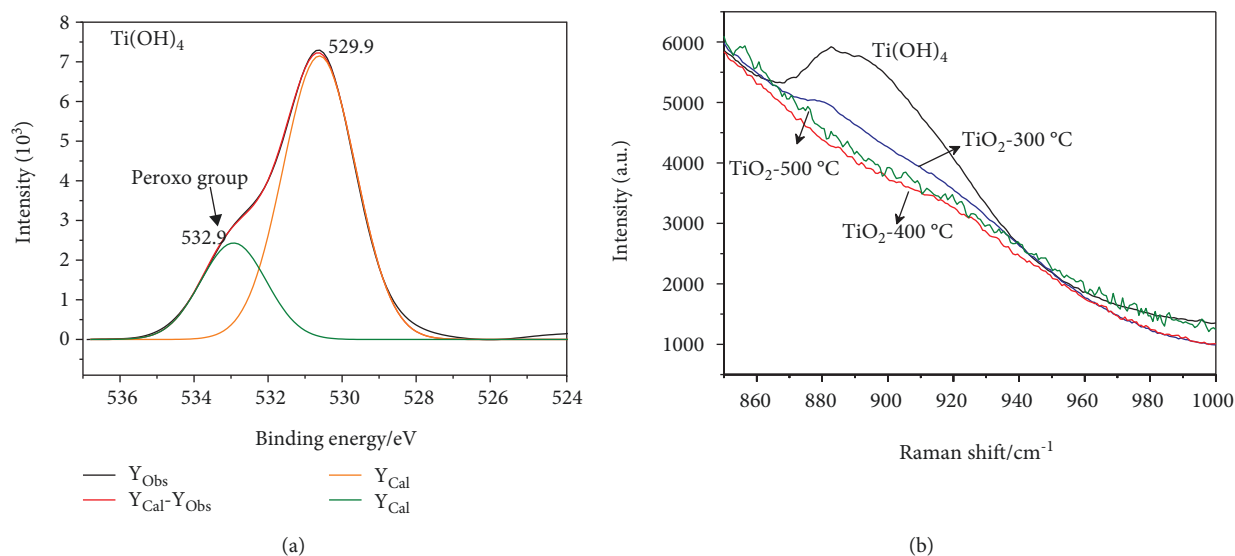


FIGURE 1: (a) XPS profile of $Ti(OH)_4$ and (b) Raman spectra of $Ti(OH)_4$ and TiO_2 powders calcined at different temperatures for 1 h.

the influence of radiation on the degradation process of organic compounds in the photocatalysis process, the same experiment was carried out without the presence of the catalyst. For the catalyst adsorption capacity test, we used the same conditions except the presence of radiation. Specified amount of reaction mixture was collected at regular time intervals and analyzed in a UV-Vis spectrophotometer (Shimadzu UV-1601 PC) in the absorbance mode monitor.

2.4. CO₂ Photoreduction. The CO₂ photoreduction tests were performed using 300 mg of the catalyst suspended in 300 mL of water in a 500 mL steel cylindrical reactor, covered with borosilicate glass. Ultrapure CO₂ was bubbled through the reactor for at least 10 min to ensure that all dissolved oxygen was eliminated. The illumination system included a UVC lamp (PHILIPS 11 W) with a wavelength of 253.7 nm in the center of the reactor, and the intensity of the incident light was 9.1 mW/cm².

The reaction progress was monitored by collecting and analyzing the sample at regular intervals. Gaseous products were determined with the help of GC-TCD and GC-FID (Varian, CP-3800) using a packed column (HayeSep N (0.5 m × 1.8")) at a flow rate of 30 mL min⁻¹ for H₂, 300 mL min⁻¹ for air, and 30 mL min⁻¹ for N₂, injector temperature of 150°C, TCD detector temperature of 200°C, and FID detector temperature of 150°C. For determining the gaseous products, a 2 μL sample was injected in the GC and then the yield was correlated by injecting a standard gaseous mixture. Blank reactions were carried out to ensure that the CH₄ originated were photoreduction products of CO₂. In the blank reaction, no catalyst was added and all other conditions were maintained the same.

3. Results and Discussion

3.1. Characterization. The synthesis of $Ti(OH)_4$ was carried out following the same principle of peroxy complex hydrolysis by the formation of water through the oxidation of H₂O₂

as reported by Ribeiro et al. and Camargo et al. [12–14]. However, in this work, instead of the oxidation process of H₂O₂ occurring through a redox reaction, the solution of peroxy-titanium complex was heated, leading to the decomposition of H₂O₂ and the formation of O₂ and H₂O, causing hydrolysis of peroxy complex and the consequent formation of the precipitate [17–20].

The surface of the $Ti(OH)_4$ was characterized by X-ray photoelectron spectroscopy (XPS), in which the XPS spectrum in the O1s region showed two peaks (Figure 1(a)). The main peak at 529.9 eV is related to the oxygen anions, O²⁻, bound to the metal cations in the lattice, and the second peak at 532.9 eV could be attributed to the formation of peroxy groups on the $Ti(OH)_4$ [20]. Raman spectra of $Ti(OH)_4$ and calcined materials are reported in Figure 1(b). The $Ti(OH)_4$ spectrum is dominated by a broad band between 880 and 940 cm⁻¹, related to the O-O stretching vibration, which is typical for peroxy groups on the surface of titanium oxide as reported by Zou et al. [21]. It was observed that calcination temperatures above 300°C cause a reduction in the amount of peroxy groups on the catalyst surface and in higher temperatures, the presence of this band no longer occurs showing the complete elimination of the groups on the material surface.

Figure 2(a) shows the TG-DTG curves of $Ti(OH)_4$. The TG curve for the $Ti(OH)_4$ showed weight loss in two stages. The first was observed between 25°C and 150°C, and the second was recorded at a temperature range from 250°C to 300°C. The weight loss in the first temperature interval could be attributed to the removal of adsorbed water in the catalyst surface. At temperatures between 250°C and 300°C, there were weight losses of 24%, which could be attributed to the peroxy groups bonded to catalyst particles.

The two weight loss regions observed in the TG are associated with one endothermic DSC peak and a few overlapped exothermic peaks (Figure 2(b)). The first weight loss of 28% was attributed to the loss of physically adsorbed water, and it could be manifested by a clear endothermic DSC peak at

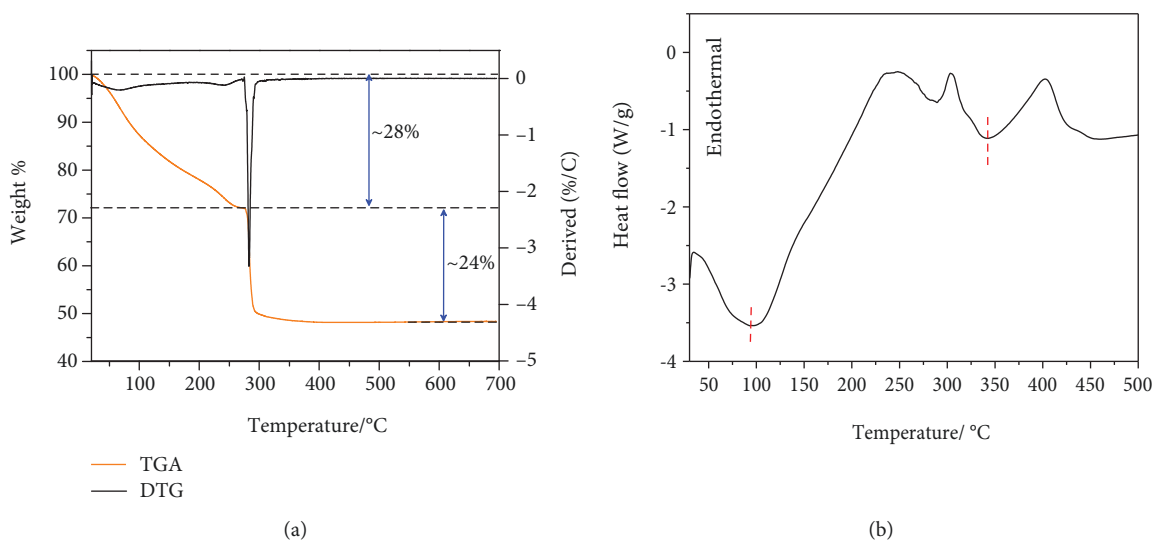


FIGURE 2: (a) TG/DTG and (b) DSC patterns of $\text{Ti}(\text{OH})_4$ powder.

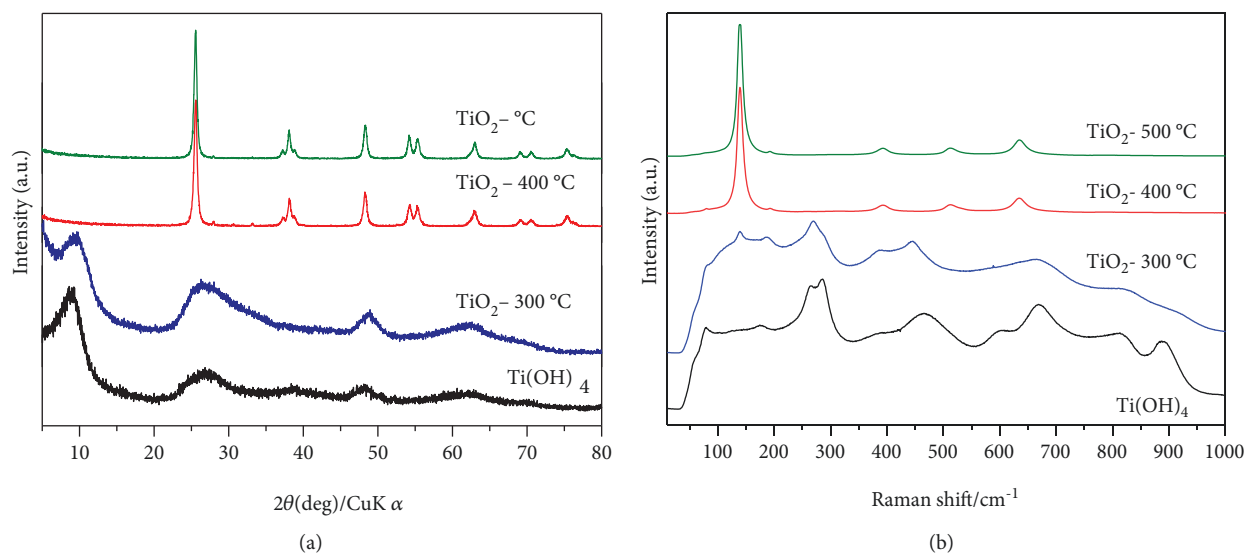


FIGURE 3: XRD patterns (a) and Raman spectroscopy of $\text{Ti}(\text{OH})_4$, TiO_2 -300°C, TiO_2 -400°C, and TiO_2 -500°C.

around 100°C. Between 200 and 500°C, a few overlapped exothermic peaks were observed in DSC accompanied by the second weight loss of 24% in the TG. These exothermic peaks might be originated from the removal of the peroxy group on the $\text{Ti}(\text{OH})_4$ surface.

The XRD patterns of the $\text{Ti}(\text{OH})_4$, TiO_2 -300°C, TiO_2 -400°C, and TiO_2 -500°C are shown in Figure 3. It can be seen from Figure 3(a) that the $\text{Ti}(\text{OH})_4$ and TiO_2 -300°C patterns show low crystalline with peaks at $2\theta = 26.5^\circ$ related to the rutile phase (JCPDS 21-1276) and $2\theta = 48.7^\circ$ and 62.2° related to the anatase phase; however, the materials calcined at 400 and 500°C presented peaks related only to the anatase phase (JCDS 21-1272). The crystallite size of the particles has been estimated from Debye-Scherrer's equation using the XRD line broadening of the (1 0 1) plane diffraction peak. In temperatures higher than 400°C, the TiO_2 starts to crystallize resulting in larger crystallites, which can be attributed to

the thermally promoted crystallite growth. The obtained crystallite sizes are shown in Table 1.

The structural properties of the materials were further investigated by Raman spectroscopy (Figure 3(b)). The samples calcined at 400 and 500°C exhibit the characteristic Raman-active modes of the TiO_2 anatase phase, in agreement with the phase composition of the materials determined by XRD [22].

In order to provide additional evidence and to confirm the effect of calcination temperatures on the $\text{Ti}(\text{OH})_4$, FTIR characterizations were performed. The infrared spectra of $\text{Ti}(\text{OH})_4$ and samples calcined at different temperatures are presented in Figure 4. The broad band at 2700–3650 cm^{-1} and the band at 1636 cm^{-1} correspond to the surface-adsorbed water and hydroxyl groups, respectively. The main band at 400–800 cm^{-1} was attributed to Ti-O stretching and Ti-O-Ti bridging stretching modes [23]. Notably, increasing

TABLE 1: Band gap energy, specific surface area, and crystallite size of the materials.

Sample	Band gap (eV)	S_{BET} ($\text{m}^2 \text{g}^{-1}$)	Crystallite size (nm)
$\text{Ti}(\text{OH})_4$	2.15	15	—
TiO_2 -300°C	2.76	45	—
TiO_2 -400°C	2.93	23	19
TiO_2 -500°C	2.88	79	20

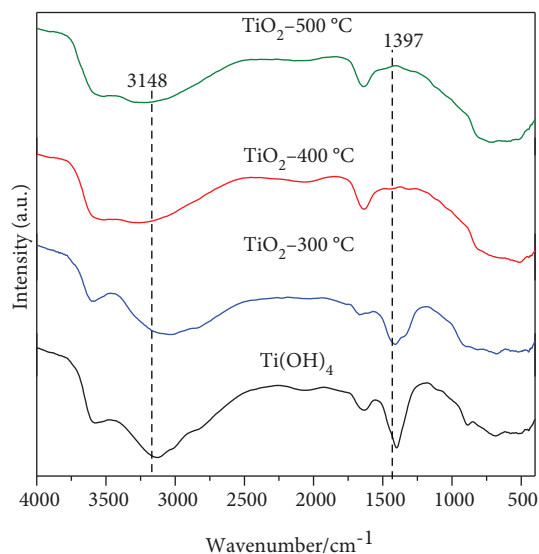


FIGURE 4: FTIR spectra of $\text{Ti}(\text{OH})_4$, TiO_2 -300°C, TiO_2 -400°C, and TiO_2 -500°C.

the temperature, the surface-adsorbed water and hydroxyl groups decreased slightly. There is no obvious characteristic band of peroxy groups on the catalyst surface, which may be limited by the detection resolution of IR.

Figure 5 shows the FEGSEM images of $\text{Ti}(\text{OH})_4$ and catalysts calcined at 300 to 500°C. It can be seen that the $\text{Ti}(\text{OH})_4$ particles are irregular in shape and have a wide particle size distribution. Most are larger than 200 nm, and it is observed that the treatment with temperature did not change the size and morphology.

The optical properties of the $\text{Ti}(\text{OH})_4$, commercial TiO_2 (TiO_2 -COM), and catalysts calcined at 300 to 500°C were examined using diffuse reflectance UV-Vis spectroscopy, and the band gap values were calculated by the Tauc method, as shown in Figure 6 [15, 16].

It is observed in the UV-Vis spectra that the increase of the calcination temperature caused a shift of the absorption edge to higher values of energy, as can be observed Figure 6. All the catalysts synthesized presented a lower band gap value than commercial titanium dioxide (Table 1).

This variation of band gap energy with increasing calcination temperature may be related to the different densities of structural and surface defects present in each of the samples. Because defects cannot be controlled in the materials, their presence only provides a change in the amount

and distribution of intermediate energy levels within the band gap region.

$\text{Ti}(\text{OH})_4$ presented a band gap energy value of 2.15 eV, with an onset of absorption from 576 nm, indicating that this catalyst is sensitive to visible light, which represents a possible photoactivity under visible radiation.

3.2. Photocatalytic Tests

3.2.1. Photodegradation. Photocatalytic studies were carried out on $\text{Ti}(\text{OH})_4$ and materials calcined at 300, 400, and 500°C and were compared with the TiO_2 -COM nanopowder (Sigma-Aldrich 99.8%) (Figure 7). To test the photocatalytic activity of the catalysts, two organic compounds were used as the pollutant model, the methylene blue dye (maximum absorption at 554 nm), and the amiloride drug (maximum absorption 286 nm) (Figure 8).

The photolysis test of the MB was carried out under UV and visible radiation under the same conditions of the photocatalysis reaction, except without the presence of a catalyst. In this study, we can observe that under UV radiation the dye presents a small degradation by this process, which indicates that the catalyst plays a key role in the degradation of MB. The catalysts were investigated by the adsorption capacities under the same conditions as the photoreduction but without the presence of radiation, in order to distinguish between the adsorption and photocatalytic phenomena (Figure S1). $\text{Ti}(\text{OH})_4$ presented the highest adsorption capacity of approximately 19% in relation to other materials; however, it is observed that the photocatalytic effect of $\text{Ti}(\text{OH})_4$ is much higher than that of other materials under visible radiation (see Supplementary Materials). It is important to note that the results are due to the combined effect of the adsorption and photocatalysis process.

Figure 7(a) shows that $\text{Ti}(\text{OH})_4$ and TiO_2 -COM were the two catalysts that showed the highest photocatalytic activity, with 100% discoloration of the solution in 60 min of reaction under UV radiation. The degradation rate becomes less pronounced when the calcination temperature used for the production of materials is increased from 300 to 500°C. On the other hand, when the reaction was conducted under visible radiation, the $\text{Ti}(\text{OH})_4$ was much more active than the other catalysts, which was expected since it has a higher absorption in the visible region compared to the other catalysts (Figure 7(b)).

One of the problems of testing photocatalytic activity of a catalyst using dye is that the sensitization process can occur [24]. This mechanism occurs when a molecule that has absorption in the visible region, such as dyes, is adsorbed on the surface of a semiconductor and is excited from its ground state (HOMO) to the excited state (LUMO), transferring these electrons to the semiconductor spontaneously, being the first stage of its oxidation. Furthermore, it can be found that amiloride is very stable under visible light radiation (Figure 8(b)), revealing that degradation does not occur without a photocatalyst. It is observed that $\text{Ti}(\text{OH})_4$ had the best photocatalytic activity, presenting 90% removal with 20 min of reaction under

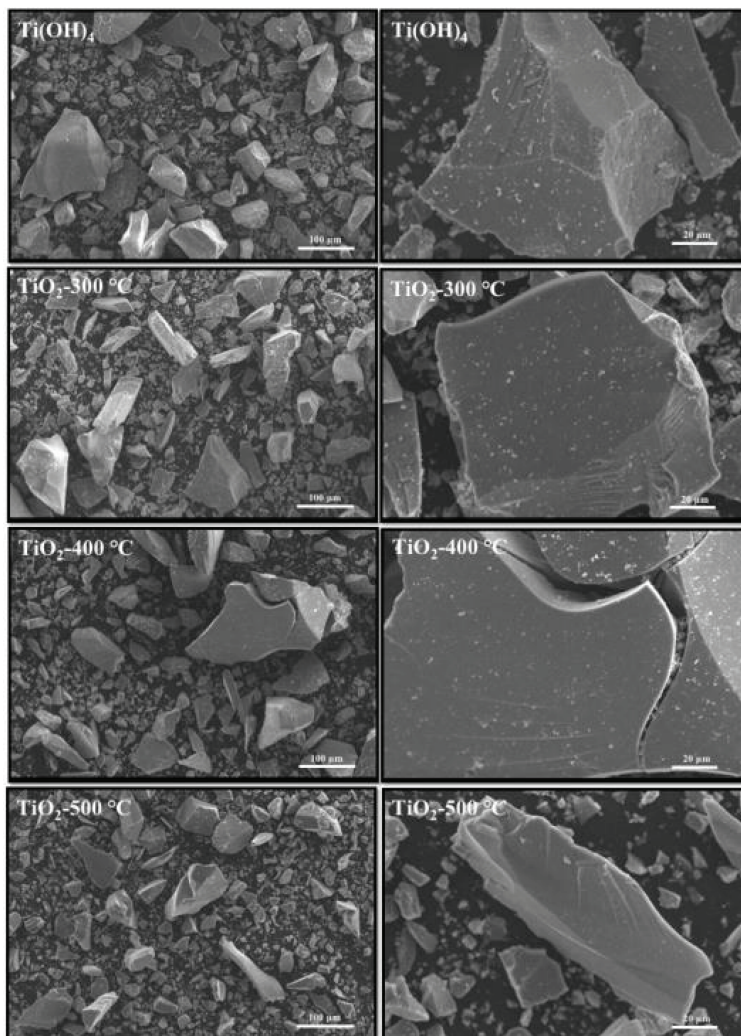


FIGURE 5: FEGSEM image of the $\text{Ti}(\text{OH})_4$ powder and the catalyst calcined at different temperatures for 1 h.

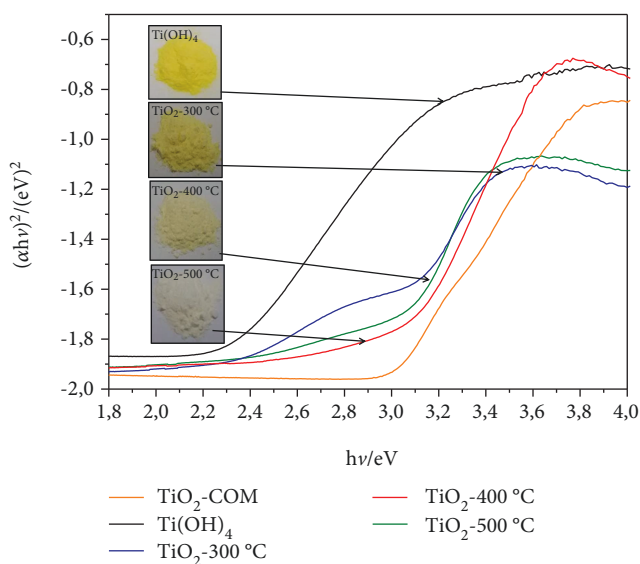


FIGURE 6: UV-Vis diffuse reflectance spectroscopy of catalysts and inset photography of materials.

visible radiation, while $\text{TiO}_2\text{-COM}$ presented only 5% of removal at this same reaction time.

These results show that the absorption edge shift of $\text{Ti}(\text{OH})_4$, due to the presence of the peroxy groups on the surface, had a great influence on the catalytic activity of the catalyst under visible radiation, where it was observed that the removal of these peroxy groups in the surface by the calcination process decreased the photocatalytic activity of these materials under visible radiation, probably due to their low absorption capacity in the visible region.

The order of reaction with respect to MB and AML degradation was determined by plotting the reaction time as a function of $\ln [C]/[C_0]$ according to the following equation for the materials:

$$\ln \left(\frac{C}{C_0} \right) = -kt, \quad (2)$$

where $[C_0]$ and $[C]$ represent the concentration of the substrate in solution at time zero and the time of illumination,

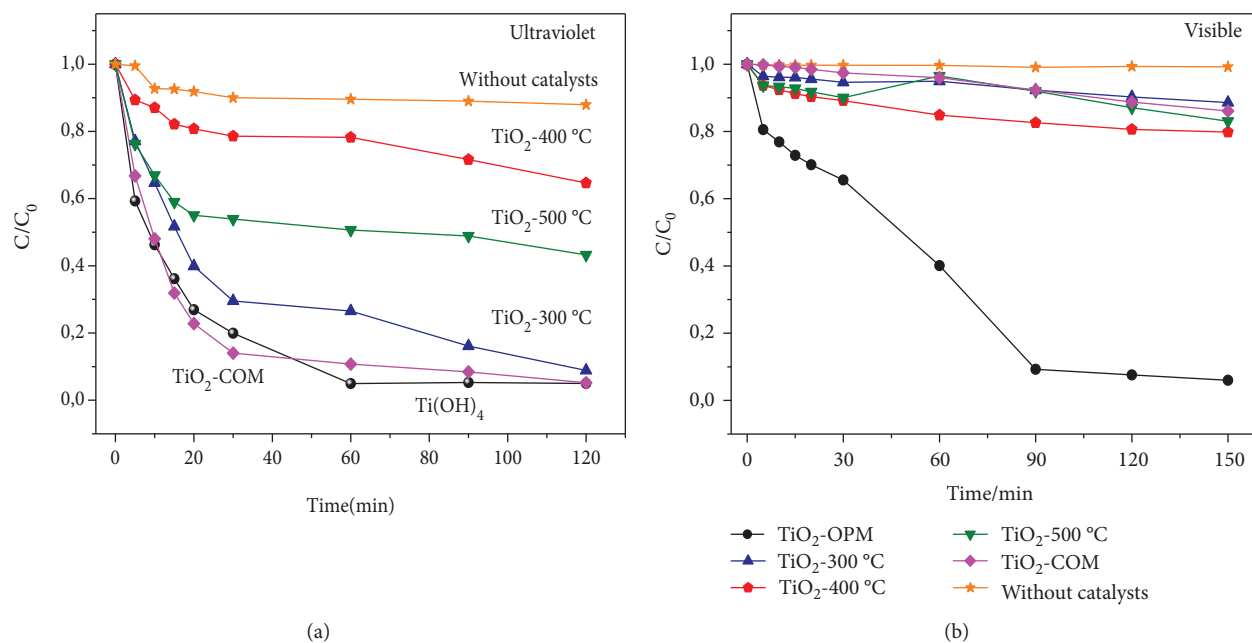


FIGURE 7: The kinetic process of MB degradation (a) under UV and (b) visible light radiation.

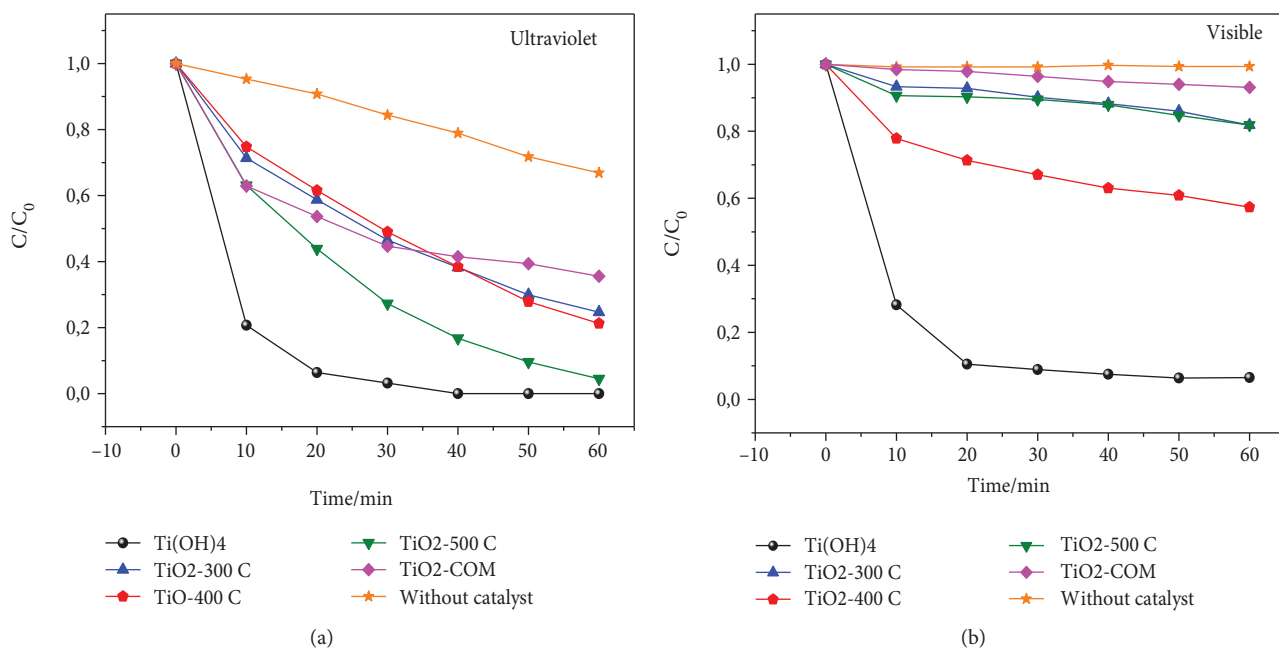


FIGURE 8: Degradation kinetics of AML (a) under UV and (b) visible light radiation in the solutions containing $Ti(OH)_4$, TiO_2-COM , $TiO_2-300^\circ C$, $TiO_2-400^\circ C$, and $TiO_2-500^\circ C$.

respectively, and k represents the apparent rate constant (min^{-1}). The apparent rate constants are summarized in Tables 2 and 3. The results show that the reaction followed first-order kinetics.

The stability of the catalyst over a photodegradation is a critical factor for its practical application. Therefore, the photostability of the $Ti(OH)_4$ sample, which showed the best photoactivity, was evaluated by performing recycling

experiments under UV irradiation (Figure S2). After each reaction cycle, the sample was separated from the MB solution by centrifugation and placed immediately in contact with a freshly prepared MB solution. This procedure was repeated four times under the same conditions used in the photocatalytic tests. As shown in Figure S2, a slight decrease (ca. 4%) occurs after the first photocatalysis cycle. In addition, the peroxy groups were analyzed after the

TABLE 2: Photocatalytic reaction constants of the MB degradation.

Material	Ultraviolet		Visible	
	$k \times 10^{-3}$ (min ⁻¹)	R ²	$k \times 10^{-3}$ (min ⁻¹)	R ²
Ti(OH) ₄	44.1	0.9777	8.26	0.9851
TiO ₂ -COM	63.3	0.9842	0.972	0.9880
TiO ₂ -300°C	39.5	0.9872	0.752	0.9292
TiO ₂ -400°C	5.30	0.8844	1.95	0.9588
TiO ₂ -500°C	20.8	0.9882	1.63	0.9575

TABLE 3: Photocatalytic reaction constants of the AML degradation.

Material	Ultraviolet		Visible	
	$k \times 10^{-3}$ (min ⁻¹)	R ²	$k \times 10^{-3}$ (min ⁻¹)	R ²
Ti(OH) ₄	114	0.9571	82	0.8713
TiO ₂ -COM	15	0.9937	1	0.9876
TiO ₂ -300°C	23	0.9949	3	0.9472
TiO ₂ -400°C	25	0.9856	8	0.8663
TiO ₂ -500°C	50	0.845	3	0.8490

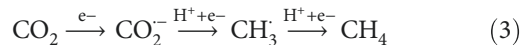
photocatalysis reaction, in which it was observed that after the reaction the groups were maintained (Figure S3).

The formation of the stable metal-peroxo group, which may be partially in equilibrium with radical metal-O₂[·] species, has been recognized to play an important role in the photocatalytic process, as these groups can inhibit the recombination of photogenerated charges and interact with photogenerated holes [25, 26]. Photogenerated valence band holes (h^+) are trapped at the surface oxygen to form the ·OH radical. On the other hand, the electrons in the conduction band can react with H₂O to form the ·OOH radical (Figure 9) [27].

Zhang and Nosaka studied the formation of the ·OH radical from TiO₂ and demonstrated that the mechanism of ·OH generation occurs differently depending on the crystalline phase of TiO₂ (Figure 9). They observed that on the surface of the rutile, ·OH is generated by the oxidation of the water through the h^+ photogenerated with the peroxo group on the surface; on the other hand, in the anatase phase, the OH is generated by the reaction of the metal-O₂[·] radical [28, 29]. This difference in the mechanism of ·OH generation occurs due to the packaging of the crystalline structure, in which the rutile phase presents a greater packaging with respect to the anatase phase, better stabilizing the peroxo group in the surface. Since the peroxo group is equivalent to the adsorbed H₂O₂, the presence of the rutile phase in Ti(OH)₄ may be favoring an increase in the generation of the ·OH radical that consequently increases its photocatalytic activity.

3.2.2. CO₂ Photoreduction. Another aspect of the photocatalysis process is the CO₂ photoreduction also known as artificial photosynthesis. Unlike the photodegradation process, which generates oxidizing radicals (·OH e ·OOH), the photoreproduction process happens with the electrons

photoexcited to the CB that are captured by the molecules of CO₂ adsorbed on the surface of the catalyst forming carbon dioxide (CO₂^{·-}) radicals, which will later lead to the formation of compounds with a higher added value such as CH₄, ethanol, and formic acid [30].



Thus, to verify the Ti(OH)₄ activity in CO₂ photoreduction, tests were performed under UV radiation in the aqueous medium (Figure 10).

A series of control experiments were conducted for quality assurance and to ascertain correct results. The first tests were performed in the dark with and without a catalyst, under the same experimental conditions as the CO₂ photoreduction. No products were detected in the two control experiments, indicating that CO₂ conversion, as described below, is a true photocatalytic reduction process.

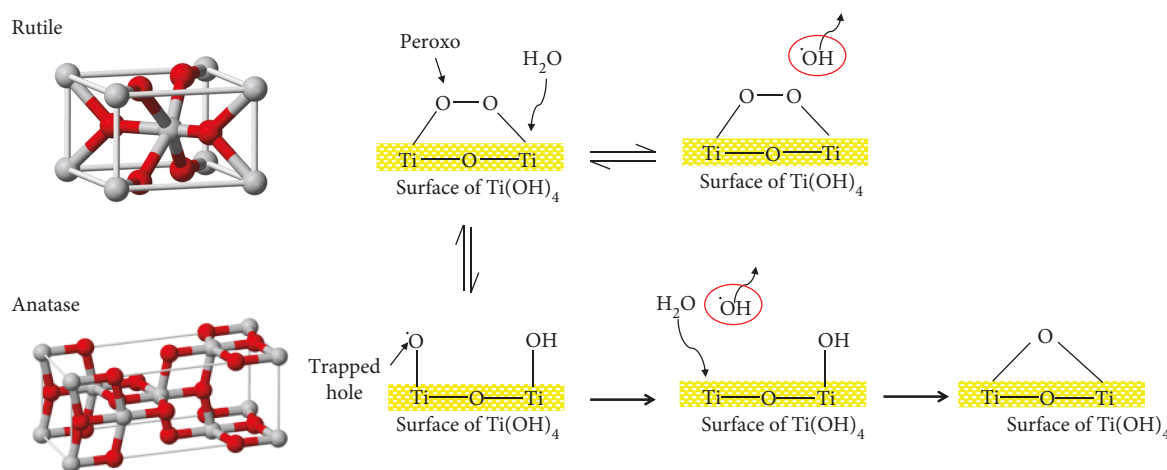
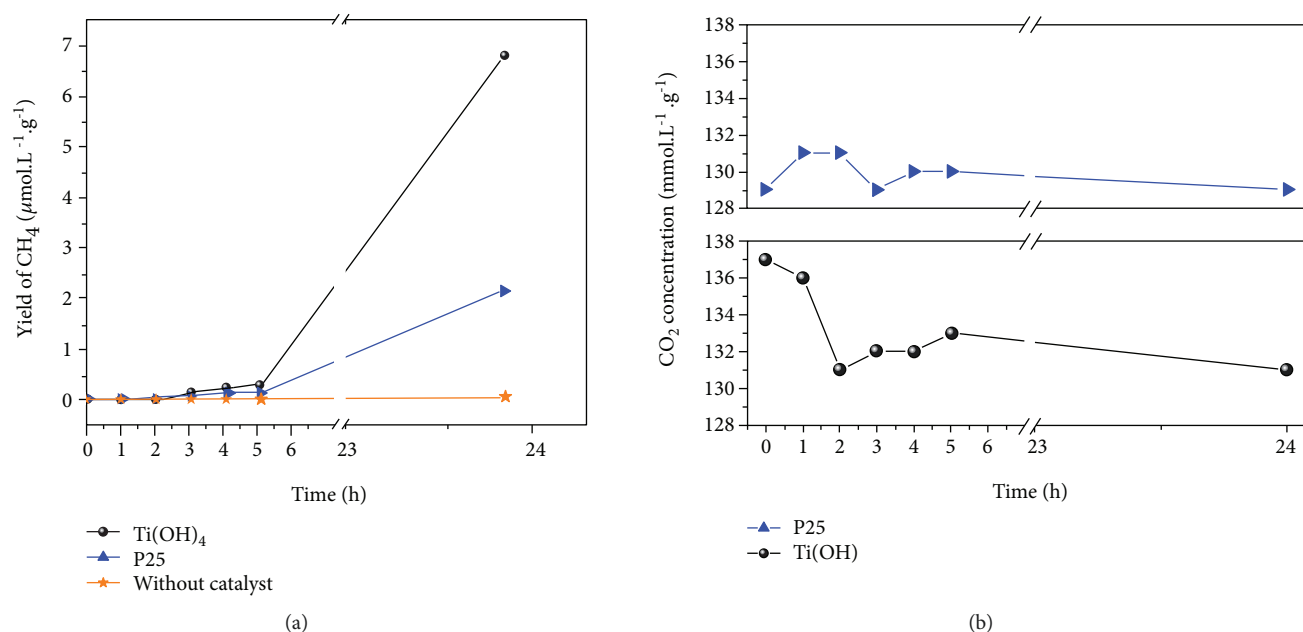
Analysis of the gas samples indicated that only CH₄ was formed using Ti(OH)₄ and the yield was 6.81 μmol·L⁻¹·g⁻¹, which was almost 3 times higher than the result obtained using P25 (2.18 μmol·L⁻¹·g⁻¹), which is the conventional catalyst used in photocatalytic processes. The concentration of CO₂ present in the gaseous medium varied during the reaction (Figure 10(b)); this variation is related to the equilibrium displacement over the photoreduction process. During the photoreduction process, the CO₂ is consumed from the aqueous medium, and in order to maintain the equilibrium, the part of the gas moves to the liquid medium causing that variation in the concentration of CO₂ in the gas phase during the reaction.

It is important to note that the CO₂ concentration variation in the gas phase was approximately 140–130 mmol·L⁻¹·g⁻¹ for all materials, indicating that, despite the small variation observed, CO₂ concentration may be considered constant during the reaction time.

4. Conclusions

The OPM route proved to be efficient in obtaining Ti(OH)₄ nanoparticles with the surface modified by peroxo groups. These groups had a great influence on the processes of photocatalysis, both in the oxidation process of organic compounds and in the photoreduction of CO₂, not only increasing the absorption of the radiation in the visible region but also providing an effective separation of photogenerated charges. We investigated the effect of the calcination temperature on the photocatalytic activity of Ti(OH)₄, and the results showed that the best result was achieved with uncalcined Ti(OH)₄, exhibiting 98% degradation of AML and MB under irradiation of visible light, being more than 10 times more active than TiO₂-COM. In addition, Ti(OH)₄ with the modified surface proved to be a good candidate for applications in CO₂ photoreduction processes.

It is important to note that the OPM method can be used to obtain other oxides such as niobium oxide, vanadium oxide, and tungsten oxide that are good candidates for applications in photocatalytic processes.

FIGURE 9: Schematic illustration of OH generation at rutile and anatase TiO₂.FIGURE 10: (a) CO₂ photoreduction kinetics and (b) CO₂ concentration as a function of irradiation time, under UVC-light.

Data Availability

No data were used to support this study.

Conflicts of Interest

The authors declare no conflict of interest.

Acknowledgments

The authors would like to thank the financial support given by FAPESP (2014/09014-7), CNPEM/LNNano, SISNANO/MCTI, and Empresa Brasileira de Pesquisa Agropecuária AgroNano research network. We also acknowledge the CDMF/CEPID.

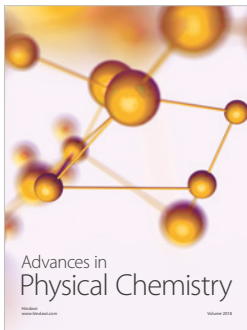
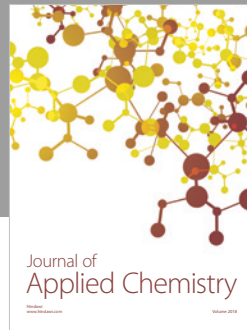
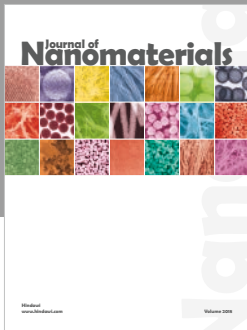
Supplementary Materials

Percentages of MB dye removal under visible light irradiation during 120 min by the combined and separated processes (adsorption and photocatalysis), recycling test of Ti(OH)₄ for the MB removal under UV radiation, and Raman spectra of Ti(OH)₄ before and after of photocatalytic process. (*Supplementary Materials*)

References

- [1] M. Pelaez, N. T. Nolan, S. C. Pillai et al., "A review on the visible light active titanium dioxide photocatalysts for environmental applications," *Applied Catalysis. B, Environmental*, vol. 125, pp. 331–349, 2012.

- [2] S. Abu-Bakar and C. Ribeiro, "An insight toward the photocatalytic activity of S doped 1-D TiO₂ nanorods prepared via novel route: as promising platform for environmental leap," *Journal of Molecular Catalysis A: Chemical*, vol. 412, pp. 78–92, 2016.
- [3] A. Mills, C. O'Rourke, and K. Moore, "Powder semiconductor photocatalysis in aqueous solution: an overview of kinetics-based reaction mechanisms," *Journal of Photochemistry and Photobiology A: Chemistry*, vol. 310, pp. 66–105, 2015.
- [4] S. M. Rodríguez, J. B. Gálvez, M. I. Maldonado Rubio, P. F. Ibáñez, W. Gernjak, and I. O. Alberola, "Treatment of chlorinated solvents by TiO₂ photocatalysis and photo-Fenton: influence of operating conditions in a solar pilot plant," *Chemosphere*, vol. 58, no. 4, pp. 391–398, 2005.
- [5] J. Mao, K. Li, and T. Peng, "Recent advances in the photocatalytic CO₂ reduction over semiconductors," *Catalysis Science & Technology*, vol. 3, no. 10, p. 2481, 2013.
- [6] A. E. Nogueira, A. R. F. Lima, E. Longo, E. R. Leite, and E. R. Camargo, "Effect of lanthanum and lead doping on the microstructure and visible light photocatalysis of bismuth titanate prepared by the oxidant peroxide method (OPM)," *Journal of Photochemistry and Photobiology A: Chemistry*, vol. 312, pp. 55–63, 2015.
- [7] M. C. Neves, J. M. F. Nogueira, T. Trindade, M. H. Mendonça, M. I. Pereira, and O. C. Monteiro, "Photosensitization of TiO₂ by Ag₂S and its catalytic activity on phenol photodegradation," *Journal of Photochemistry and Photobiology A: Chemistry*, vol. 204, no. 2-3, pp. 168–173, 2009.
- [8] H. J. Yun, H. Lee, J. B. Joo, N. D. Kim, M. Y. Kang, and J. Yi, "Facile preparation of high performance visible light sensitive photo-catalysts," *Applied Catalysis. B, Environmental*, vol. 94, no. 3-4, pp. 241–247, 2010.
- [9] J. Wen, X. Li, W. Liu, Y. Fang, J. Xie, and Y. Xu, "Photocatalysis fundamentals and surface modification of TiO₂ nanomaterials," *Chinese Journal of Catalysis*, vol. 36, no. 12, pp. 2049–2070, 2015.
- [10] W. Macyk, K. Szaciłowski, G. Stochel, M. Buchalska, J. Kuncewicz, and P. Łabuz, "Titanium(IV) complexes as direct TiO₂ photosensitizers," *Coordination Chemistry Reviews*, vol. 254, no. 21-22, pp. 2687–2701, 2010.
- [11] R. Abe, K. Sayama, and H. Arakawa, "Dye-sensitized photocatalysts for efficient hydrogen production from aqueous I⁻ solution under visible light irradiation," *Journal of Photochemistry and Photobiology A: Chemistry*, vol. 166, no. 1-3, pp. 115–122, 2004.
- [12] C. Ribeiro, C. M. Barrado, E. R. de Camargo, E. Longo, and E. R. Leite, "Phase transformation in titania nanocrystals by the oriented attachment mechanism: the role of the pH value," *Chemistry - A European Journal*, vol. 15, no. 9, pp. 2217–2222, 2009.
- [13] E. R. Camargo, J. Frantti, and M. Kakihana, "Low-temperature chemical synthesis of lead zirconate titanate (PZT) powders free from halides and organics," *Journal of Materials Chemistry*, vol. 11, no. 7, pp. 1875–1879, 2001.
- [14] E. R. Camargo, M. Popa, J. Frantti, and M. Kakihana, "Wet-chemical route for the preparation of lead zirconate: an amorphous carbon- and halide-free precursor synthesized by the hydrogen peroxide based route," *Chemistry of Materials*, vol. 13, no. 11, pp. 3943–3948, 2001.
- [15] D. L. Wood and J. Tauc, "Weak absorption tails in amorphous semiconductors," *Physical Review B*, vol. 5, no. 8, pp. 3144–3151, 1972.
- [16] L. Tolvaj, K. Mitsui, and D. Varga, "Validity limits of Kubelka-Munk theory for DRIFT spectra of photodegraded solid wood," *Wood Science and Technology*, vol. 45, no. 1, pp. 135–146, 2011.
- [17] E. R. Camargo, M. G. Dancini, and M. Kakihana, "The oxidant peroxo method (OPM) as a new alternative for the synthesis of lead-based and bismuth-based oxides," *Journal of Materials Research*, vol. 29, no. 01, pp. 131–138, 2014.
- [18] F. P. Cardoso, A. E. Nogueira, P. S. O. Patrício, and L. C. A. Oliveira, "Effect of tungsten doping on catalytic properties of niobium oxide," *Journal of the Brazilian Chemical Society*, vol. 23, no. 4, 2012.
- [19] D. Bayot and M. Devillers, "Peroxo complexes of niobium(V) and tantalum(V)," *Coordination Chemistry Reviews*, vol. 250, no. 19-20, pp. 2610–2626, 2006.
- [20] P. Francatto, F. N. Souza Neto, A. E. Nogueira et al., "Enhanced reactivity of peroxo-modified surface of titanium dioxide nanoparticles used to synthesize ultrafine bismuth titanate powders at lower temperatures," *Ceramics International*, vol. 42, no. 14, pp. 15767–15772, 2016.
- [21] J. Zou, J. Gao, and F. Xie, "An amorphous TiO₂ sol sensitized with H₂O₂ with the enhancement of photocatalytic activity," *Journal of Alloys and Compounds*, vol. 497, no. 1-2, pp. 420–427, 2010.
- [22] H. C. Choi, Y. M. Jung, and S. B. Kim, "Size effects in the Raman spectra of TiO₂ nanoparticles," *Vibrational Spectroscopy*, vol. 37, no. 1, pp. 33–38, 2005.
- [23] A. N. Murashkevich, A. S. Lavitskaya, T. I. Barannikova, and I. M. Zharskii, "Infrared absorption spectra and structure of TiO₂-SiO₂ composites," *Journal of Applied Spectroscopy*, vol. 75, no. 5, pp. 730–734, 2008.
- [24] B. Ohtani, "Great challenges in catalysis and photocatalysis," *Frontiers in Chemistry*, vol. 5, 2017.
- [25] A. E. Nogueira, T. C. Ramalho, and L. C. A. Oliveira, "Photocatalytic degradation of organic compound in water using synthetic niobia: experimental and theoretical studies," *Topics in Catalysis*, vol. 54, no. 1-4, pp. 270–276, 2011.
- [26] T. C. Ramalho, L. C. A. Oliveira, K. T. G. Carvalho, E. F. Souza, E. F. F. da Cunha, and M. Nazzaro, "Catalytic behavior of niobia species on oxidation reactions: insights from experimental and theoretical models," *Journal of Materials Science*, vol. 43, no. 17, pp. 5982–5988, 2008.
- [27] A. Ajmal, I. Majeed, R. N. Malik, H. Idriss, and M. A. Nadeem, "Principles and mechanisms of photocatalytic dye degradation on TiO₂ based photocatalysts: a comparative overview," *RSC Advances*, vol. 4, no. 70, pp. 37003–37026, 2014.
- [28] J. Zhang and Y. Nosaka, "Mechanism of the OH radical generation in photocatalysis with TiO₂ of different crystalline types," *Journal of Physical Chemistry C*, vol. 118, no. 20, pp. 10824–10832, 2014.
- [29] Y. Nosaka, "Surface chemistry of TiO₂ photocatalysis and LIF detection of OH radicals," in *Environmentally Benign Photocatalysts*, Nanostructure Science and Technology, M. Anpo and P. Kamat, Eds., Springer, New York, NY, 2010.
- [30] A. Nikokavoura and C. Trapalis, "Alternative photocatalysts to TiO₂ for the photocatalytic reduction of CO₂," *Applied Surface Science*, vol. 391, pp. 149–174, 2017.



Hindawi

Submit your manuscripts at
www.hindawi.com

